Transient Dynamics versus Fixed Points in Odor Representations by Locust Antennal Lobe Projection Neurons

Ofer Mazor[1] and Gilles Laurent*
Computation and Neural Systems Program
Division of Biology
California Institute of Technology
Pasadena, California 91125

Summary

Projection neurons (PNs) in the locust antennal lobe exhibit odor-specific dynamic responses. We studied a PN population, stimulated with five odorants and pulse durations between 0.3 and 10 s. Odor representations were characterized as time series of vectors of PN activity, constructed from the firing rates of all PNs in successive 50 ms time bins. Odor representations by the PN population can be described as trajectories in PN state space with three main phases: an on transient, lasting 1–2 s; a fixed point, stable for at least 8 s; and an off transient, lasting a few seconds as activity returns to baseline. Whereas all three phases are odor specific, optimal stimulus separation occurred during the transients rather than the fixed points. In addition, the PNs' own target neurons respond least when their PN-population input stabilized at a fixed point. Steady-state measures of activity thus seem inappropriate to understand the neural code in this system.

Introduction

Mapping and coding schemes in the brain are the subjects of considerable interest in neuroscience. Experimental and theoretical work in several systems has addressed both the density (Duchamp-Viret et al., 1996; Fiete et al., 2004; Fitzpatrick et al., 1997; Hahnloser et al., 2002; Olshausen and Field, 2004; Pouget et al., 1999; Vinje and Gallant, 2000) and the dynamical structure (Aksay et al., 2001; Buzsaki and Draguhn, 2004; Freeman, 2000; Hahnloser et al., 2002; Mao et al., 2001; Skaggs and McNaughton, 1996; VanRullen et al., 2005) of neural population activity. In recent years, similar issues have started being addressed in the early olfactory system of vertebrates and invertebrates alike (Axel, 1995; Buck and Axel, 1991; Dulac, 1997; Laurent, 1999). Current issues of debate regarding olfactory coding principles include two related aspects: (1) the density of representations across the principal neurons of the first population (mitral cells in the olfactory bulb), and (2) the stationarity of these representations over the duration of a single odor sample (e.g., a sniff). The issue of representation density is well illustrated by recent studies of the rodent olfactory bulb (OB). Electrophysiological evidence from anaesthetized animals suggests very sparse odor representations by small groups of highly specific mitral cells (Lin et al., 2005). Nevertheless, behavioral

studies of odor discrimination in animals with large OB lesions (Slotnick and Bodyak, 2002) suggest that representations may be more distributed. The issues of dynamics and stationarity, although not new (Adrian, 1953; Kauer and Moulton, 1974; Macrides and Chorover, 1972), are also well illustrated by examples from recent literature. In the zebrafish OB, odor representations by mitral cells evolve over time, such that an observer can perform better discrimination if those representations are studied piecewise and allowed to evolve over a few hundred milliseconds (Friedrich and Laurent, 2001). Recent evidence from rodents trained to discriminate between related odors indicates that at least under one set of training and testing conditions, decisions are routinely made within 200–300 milliseconds (Abraham et al., 2004; Uchida and Mainen, 2003). These results put time constraints on the optimization of odor representations by circuit dynamics.

These same issues have been examined recently in the olfactory systems of several insects, including the fruit fly (Wang et al., 2003; Wilson et al., 2004), the moth *Manduca sexta* (Christensen et al., 2000; Daly et al., 2004), and the honeybee (Fdez Galan et al., 2004; Sachse and Galizia, 2002). Our present study addresses these issues in the antennal lobes and mushroom bodies of the locust. In the antennal lobe, odors are represented by groups of projection neurons (PNs), the functional analogs of vertebrate mitral cells. There are 830 PNs in the locust antennal lobe. These PNs project to the mushroom body, where they contact a large population of neurons called Kenyon cells (50,000 in the locust). Recent work shows that although representations of odors by PNs are distributed and dynamic, they are very sparse and specific in the mushroom body (Perez-Orive et al., 2002, 2004; Stopfer et al., 2003). The cellular, synaptic, and circuit mechanisms underlying this transformation have been studied in some detail (R.A. Jortner, S.S. Farivar, G.L., unpublished data; Perez-Orive et al., 2004; Perez-Orive et al., 2002). In the present study, we analyze in quantitative depth the nature of odor representations by the PN population with a sample of 99 PNs (out of 830 in toto), five odors, and four odor pulse durations. Our goal was to characterize the statistical features of these representations. How many PNs are activated over one single oscillation cycle of a long-lasting response? How reliable are the spikes produced by activated PNs? How rapidly do the representations evolve, and does that speed change with time? Do representations eventually stabilize, and if so, do those stabilized representations represent an optimum of discriminability?

The answers to these types of questions are critical to a deep understanding of any population code, especially one associated with a sensory system. The locust olfactory system is one of the few current experimental systems that can provide quantitative answers to many of these questions. Our present results indicate that odor representations by the PN population contain both dynamic and static phases (when odor pulses are longer than 1.5–2 s); yet only the dynamic phases seem functionally relevant. This appears to be true because steady

*Correspondence: laurentg@caltech.edu
[1]Present address: Department of Molecular and Cellular Biology, Harvard University, 16 Divinity Avenue, Cambridge, MA 02138.
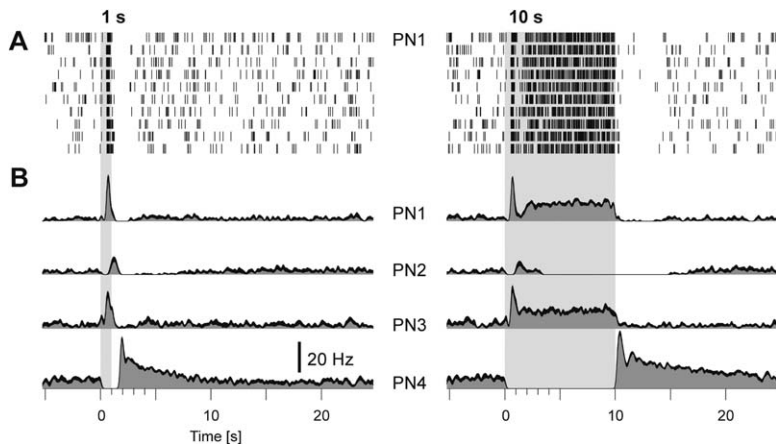
Figure 1. Slow Dynamics in Projection Neuron Responses Last Only a Few Seconds during Prolonged Odor Stimuli

(A) Ten single-trial responses of one projection neuron (PN) to 1 s and 10 s presentations of the same odor (*oct*). Each row corresponds to one trial; each tick represents the timing of one action potential from the PN. Trials of the two odor durations were interleaved.

(B) Post stimulus time histograms (PSTHs) of the PN in (A) and three other PNs in response to 1 s and 10 s odor presentations (*oct*, PN1, PN3; *cit*, PN2; *cis*, PN4). PSTHs are averages of ten single-trial responses, smoothed with a 100 ms Gaussian filter. Thickness of PSTH trace represents ± SE. Note that in all cases, the response to the 10 s stimulus reaches a constant firing rate after ~2–3 s.

state is characterized by a decrease in odor specificity (compared to the transient phases) and a lack of responsiveness of the PNs' target neurons.

Results

Odor-Evoked Dynamics

Previous studies (Laurent and Davidowitz, 1994; Laurent et al., 1996; Wehr and Laurent, 1996) revealed two general features of the odor responses of individual projection neurons (PNs) in the locust antennal lobe (AL). The first is an odor- and PN-specific pattern of excitation and inhibition, with modulations on a timescale of hundreds of milliseconds (slow dynamics). The second is the tendency of PN spikes to phase lock to the odor-evoked ~20 Hz LFP oscillation (fast dynamics). Here, we explore and quantify the progression of the slow dynamics over time by measuring the responses of a population of 99 PNs to five odors and to stimuli of varying durations (0.3–10 s).

PNs were recorded extracellularly in vivo with tetrodes (Pouzat et al., 2002). Population data were assembled by combining sets of simultaneously recorded PNs across experiments, as previously described (Stopfer et al., 2003). PNs are the only neurons of the locust antennal lobe that produce sodium action potentials (Laurent and Davidowitz, 1994). Their identification as PNs is, thus, without ambiguity.

Figure 1A shows, on a compressed time scale, the responses of one PN to 1 s and 10 s long pulses of the same odor over ten trials. Figure 1B shows the PSTH constructed from ten trials for this and three other PNs and odors. As described previously (Laurent and Davidowitz, 1994; Laurent et al., 1996; Wehr and Laurent, 1996), these individual PNs respond to a 1 s odor pulse with a period of slow dynamics lasting ~2–3 s. When the same odor is presented for 10 s, however, the slow dynamics do not last for the entire duration of the odor pulse. Instead, after 1–2 s of modulated activity (initially similar to that evoked by the shorter pulses), PN responses reach a noisy steady state, different across PNs for one odor and across odors for one PN. This steady state is often 0 Hz (i.e., lower than baseline activity) as with PN2 (Figure 1B). At the odor-pulse offset, dynamics resume: PNs inhibited at steady state return to baseline levels, either monotonically (e.g., PN2, Figure

1B) or after an overshoot of excitation (e.g., PN4, Figure 1B). PNs excited at steady state return to baseline, often after a period of inhibition (e.g., PN1, Figures 1A and 1B).

To quantify this behavior across the PN population, we measured the statistics of PN firing throughout responses to odor pulses of 0.3, 1, and 3 s durations. We chose 3 s as the longest pulse because steady state was usually reached by that time (see below). Data were taken from 99 PNs, stimulated with five odors (hexanol, cis-3-hexen-1-ol, 1-octanol, citral, and methyl salicylate) diluted in mineral oil to 1% of saturated vapor pressure. Responses were computed from nine trials per stimulus condition, representing a total of 4455 rasters (99 PNs × five odors × nine trials). The mean baseline PN firing rate calculated with this dataset was 2.6 spikes/s. Just after odor onset and odor offset, the mean firing rate rose to ~four spikes/s. Between onset and offset, the mean PN firing rate was in between baseline and this peak (Figure 2A).

The odor responses of individual PNs (e.g., Figure 1B) indicated that PNs may be strongly excited or inhibited at specific times during a response. Mean firing rates, averaged over the population (Figure 2A), thus fail to characterize the full diversity and range of activation patterns across the PN population. To address this issue, we measured the response of each PN during and around the odor trial with 50 ms time bins. Because PNs rarely generate more than one or two action potentials in a 50 ms window, we chose to study trial-to-trial reliability of each cell's activity (rather than firing rate). Response was measured as follows: each trial was divided into successive 50 ms time bins, aligned at odor pulse onset. The number of spikes produced by each PN in each time bin was measured, and a PN was described as responding during time bin *i* if it produced at least one action potential in that bin over six or more of the nine trials tested. This measure ensured that PN responsiveness was essentially 0 prior to odor onset (PN firing at baseline is 2.6 Hz and is not locked to the stimulus; it is thus unreliable from trial to trial) (Figure 2B). This measure detected reliable PN firing (with 50 ms resolution) evoked by odors. PN responses measured in this way are shown in Figure 2B: each dot indicates for each PN-odor pair (each row) whether this PN responded during the corresponding time bin.
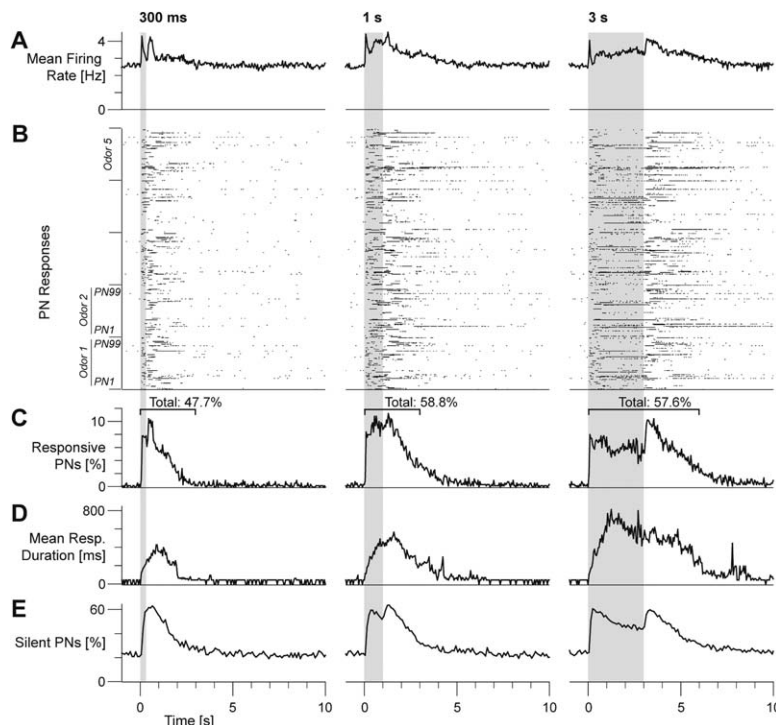
Figure 2. PN-Population Response Consists of Small, Time-Varying Subsets of Responsive PNs and a Large Fraction of Silent PNs

(A–D) All statistics were computed from 99 PNs; each presented nine times with five different odors at three different durations (300 ms, 1 s, and 3 s). Silent PNs were computed with consecutive, nonoverlapping 100 ms bins; all other statistics were computed with consecutive, nonoverlapping 50 ms bins. (A) The mean PN firing rate over all PNs and all odors, for three different odor durations (gray bars). (B) Raster plot for all PNs and all odors, indicating time bins when PNs responded (see text for definition). Each dot indicates a reliable response in a given time bin. (C) Percentage of responsive PN-odor pairs (as defined in text) over all 50 ms time bins. (D) Mean response duration for all PNs responding at each time bin (calculated separately for all time bins).

(E) Percentage of silent PNs for each time bin. A PN is defined as silent during a 100 ms time bin if it fired no spikes in that time bin in all nine stimulus trials.

The percentage of responding PNs (as defined above) during each time bin is plotted in Figure 2C. At rest, fewer than 1% of all PNs produced action potentials at a rate high enough to be detected as responding by our measure. After odor onset, however, the percentage of responsive PNs immediately rose to between 8% and 10%. For each odor pulse condition, this level of instantaneous activity persisted until about one second after odor offset, when it gradually returned to its baseline level over several seconds.

Just as there are periods of reliable PN activity (responses), there are periods of reliable odor-evoked inhibition. We measured the percentage of PNs that fired no action potentials within each 100 ms time bin (across nine trials). Time bins of 100 ms were used (as opposed to 50 ms) to allow a more conservative measure of silence. At rest, this value was 23.2%. Just after odor onset and offset, the silent population tripled to about 60% (Figure 2E). In the middle of the 3 s odor presentation, the percentage fell to ~50%.

This analysis revealed that during each 50 ms bin after odor onset, no more than 10% of the PNs are reliably active and that about 60% of the PNs are silent (Figures 2C and 2E). The remaining 30% of PNs had unreliable responses, or else were firing at random, unaffected by the odor. Of all the spikes produced during each time bin, however, 55% were due to the reliably responding PNs (i.e., to only ~10% of all PNs per time bin). This shows that during a single odor trial, more than half of all spikes produced in each 50 ms time bin originate from only 10% of all PNs but that the action of these spikes may be combined with that of other spikes produced less reliably. Hence, for each time bin, 55% of all spikes have a reliable origin, whereas the remaining 45% can be expected to be generated from a larger population of unre-

liable sources. This observation will be important when we consider the decoding of the PN population.

Because individual PNs are responsive for only a fraction of the total odor response, the identities of responding PNs change from time bin to time bin. We thus calculated the cumulative proportion of responding PNs during an odor response (over 3 s for 0.3 and 1 s pulses, over 6 s for 3 s pulses). We found that on average, 50%–60% of PNs (Figure 2C) can be described as responding at some time over the entire population response duration. This confirms that odor representations are broadly distributed across the PN population; because only 10% of PNs are coactive during any 50 ms time bin, activity must evolve across the PN population.

Accordingly, we measured the mean response duration of all responding PNs as a function of time during odor responses (Figure 2D). For example, the mean response duration during the first second of the response to a 3 s odor pulse is 370 ms. One second later, the mean response duration is 690 ms, even though the percentage of responding PNs per time bin is about the same (Figure 2C). This suggests that the speed at which PNs are being replaced slows down as the response evolves. This will be measured later.

Taken together, these data show that unlike during baseline, each time bin of the odor response is characterized by a large fraction (~60%) of silent PNs and a small and evolving subset of reliably responding PNs. The remaining projection neurons are only moderately active, spiking occasionally but not with enough consistency to meet our response criterion. Nevertheless, when the entire duration of the response is considered, about half of the PNs respond during at least one 50 ms time bin and for a few hundred milliseconds on average and therefore contribute to the population representation.
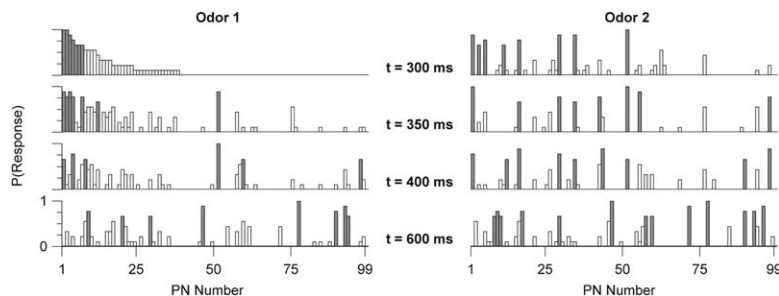
Figure 3. Selected Examples of Single-Time-Bin, Odor-Evoked PN-Population Responses

The response probabilities of all 99 PNs are displayed, for four different 50 ms time bins (t = 300, 350, 400, and 600 ms) and in response to two different odors (odor 1, cis-3-hexen-1-ol; odor 2, 1-hexanol). *P(Response)* is defined as the fraction of trials in which a PN fired at least one spike in that particular time bin. The PNs are ordered according to their response probabilities in the first time bin of odor 1 (t = 300 ms). PNs that meet our response criterion (response in at least six out of nine trials) are shaded gray. Note that the responsive PNs distribute rapidly across the population and are different across the two odors.

An example of this behavior is shown in Figure 3. The level of activity of all 99 PNs is displayed (bins 1–99) for four different 50 ms time bins (rows) and in response to two different odors. Activity (*P(Response)*) is measured as the fraction of trials in which a PN fired at least one spike in a particular time bin. The PNs are ordered according to their activity in the first time bin of odor 1 (t = 300 ms). In that first time bin of odor 1, seven of 99 PNs met our response criterion by firing spikes in at least 66% of the trials, and 61 PNs were silent, not firing a single spike in all nine trials. 50 ms later (t = 350 ms), activity across the PNs has changed slightly, though most of the responsive PNs in this time bin were also responsive in the previous time bin. After 300 ms (t = 600 ms), the set of responsive and silent PNs is seemingly unrelated to the original one (t = 300 ms). In addition, at each time bin, the subset of PNs responsive to odor 2 is different from that responsive to odor 1. We will now quantify the differences between the PN-population responses across odors and over time.

Spatio-Temporal Patterns as Trajectories in PN Space

The locust antennal lobe contains approximately 800 PNs (Laurent, 1996; Leitch and Laurent, 1996). The activity of this population of PNs at a given time can be represented as a point in an 800-dimensional space, in which each dimension represents the firing rate of one of the 800 PNs at that time. When an odor is presented, subsets of PNs are activated in a PN- and odor-specific manner, as described above. If the instantaneous firing rates of the PNs are measured over short time bins (e.g., 50 ms), the state of the PN populations should describe odor-specific trajectories, beginning and ending at a point (or cluster of points) that represents baseline activity. The following analysis examines the structure and similarity of these trajectories for different odors and stimulus durations with data gathered from 99 PNs recorded from ten antennal lobes. The 99-dimensional data were analyzed with PCA (see Experimental Procedures) and projected in the space of the first three principal components to allow visualization (Figure 4).

Figure 4A shows trajectories representing the evolution of the PN-population response to three different stimulus durations (300 ms, 1 s, and 3 s) of the same odor (1-octanol). Each point along the trajectory represents the instantaneous PN activity vector averaged over nine trials (trials 2–10), calculated here in 100 ms

bins, over an 8.5 s window around the odor presentation. The thick segments of the trajectories represent the epochs during which the stimulus was present. The thin segments represent the baseline period before odor onset and the evolution of the population response after odor termination, including the relaxation to baseline. These plots illustrate several important points that will be examined quantitatively later. First, for each odor, the initial excursions following the onsets of different duration stimulus pulses overlapped each other (with some noise) for obvious reasons. Second, the relaxation to baseline after odor offset followed trajectories different from those after odor onset: the system does not "retrace its steps" back to rest (Stopfer et al., 2003). Third, the system reached a fixed point (*FP*) only for stimulus durations longer than about 2 s (fourth frame of 3 s odor series) (Figure 4A).

The trajectories defined by the system over 7.5 s after each of the three pulse durations are superimposed in Figure 4B (*oct*). Although, as noted above, the original excursions overlapped well, the return paths to baseline were also quite similar, despite differences in past histories. This can be seen quite clearly for the trajectories defined for two other odors (*cis*, *meth*) (Figure 4B). This suggests that off-transients (i.e., segments of trajectories defined after odor offset) contain odor-specific information independent of stimulus duration.

Next, the fixed points reached by the PN population differed across odors (Figure 4C) and thus contained stimulus related information. We observed, however, that the fixed points were not necessarily the points of greatest intertrajectory separation; greater separations usually occurred during the transient (onset and offset) phases, when dynamics are seen in PN response patterns. Finally, we calculated single-trial PN vectors and superimposed the corresponding trajectories computed for all nine trials with one odor (citral) (Figure 4D). While illustrating the reliability of the odor-evoked trajectories, this plot also shows that the intertrial distances among odor-evoked trajectories were no greater during the transient phases or the odor-evoked fixed point (*FP*) than they were at rest (baseline, *B*).

To quantify these qualitative observations, we calculated the mean state of the system at rest (by averaging baseline PN activity vectors, calculated in the full 99-dimensional space, over all trials and all 50 ms long time bins in the 4 s prior to the odor presentation); we then measured the Euclidian distance from that mean
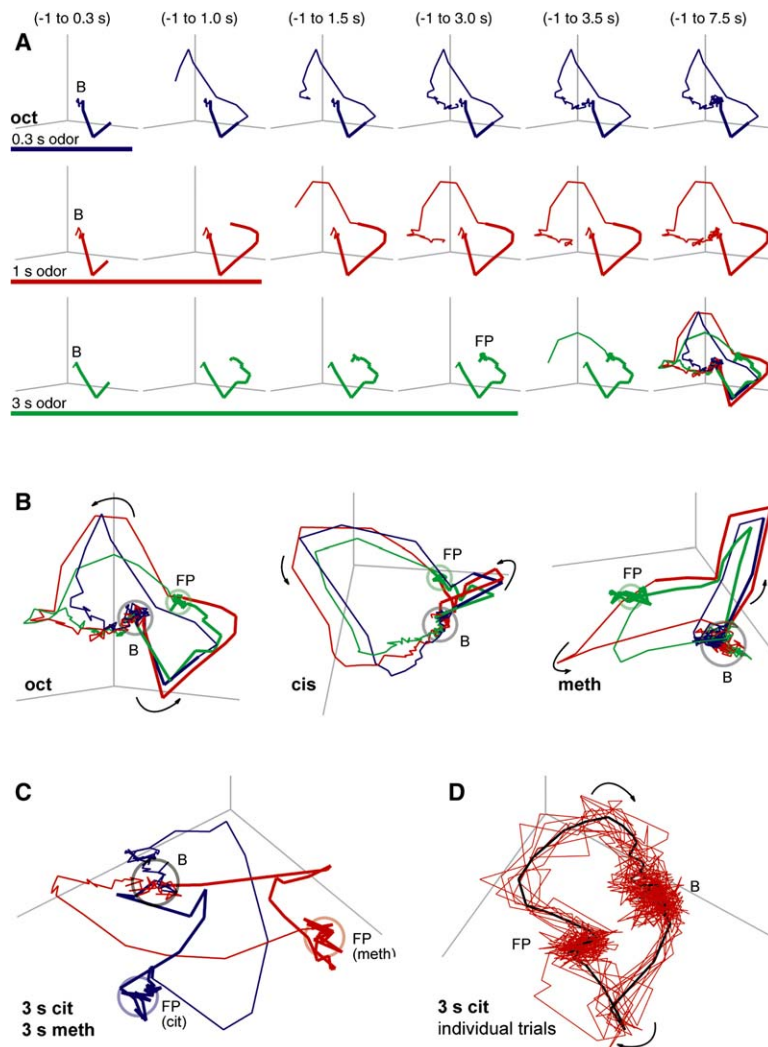
Figure 4. Visualization of PN-Population Odor Responses

The activity of the population of PNs at a given time is represented as a point in 99-dimensional space, in which each dimension represents the firing rate of one of the 99 PNs in the corresponding time bin. The 99-dimensional data were analyzed with PCA (see Experimental Procedures) and projected in the space of the first three principal components to allow visualization. (A) The population response to odorant 1-octanol at three different odor durations (blue, 300 ms; red, 1 s; green, 3 s). Activity at successive time points is joined by a line to better display the odor-evoked trajectory. The thick segments of the trajectories represent the epochs during which the stimulus was present. The thin segments represent one second of preodor baseline activity (B) as well as the evolution of the population response after odor termination, including the relaxation to baseline. All subplots use the same three principal components (PCs). The successive plots in each row represent increasingly long time frames of the response evolution. FP, fixed point. (B) Comparison between response trajectories to three different stimulus durations for three different odors (1-octanol, citral, and methyl salicylate). Principal components were computed separately for each odor. Arrows, direction of motion. (C) Odor trajectories (3 s duration) for two different odors (citral and methyl salicylate) plotted in the same PC axes (a single set of PCs was computed for all points of both odor trajectories). The fixed point (FP) for each odor is outlined by a colored circle. Note that the trajectories for both odors (including fixed points) are separate and nonoverlapping (the crossover points in the trajectories are projection artifacts: the system rarely visited the same point for two different odors). (D) Example of trial-to-trial variability. The trajectories for all nine trials of the 3 s citral presentation (red traces) are plotted, along with their mean (black trace), in their first three PC axes.

baseline PN vector to each point along each odor trajectory. The mean value of this distance (averaged over all five odors presented) is plotted in Figure 5A. In Figure 5B, we plot the mean intertrajectory distance at each time point around and during the odor response, averaged across all ten pairwise combinations of odor-specific trajectories. Taken together, these two figures show that the odor-evoked PN-population activity is most different from baseline and from other odor responses just after the onset or the offset of the odor pulse. Both intertrajectory distance and distance to baseline peaked around 100 ms after odor onset. At odor offset, both distance measures peaked after 250–300 ms (250 ms for 300 ms and 3 s odor-pulse durations, 300 ms for 1 s odor pulse). In the time between the onset and offset peaks, both distance measures decreased but remained above baseline, indicating that odors could still be identified. In the trials long enough to allow the odor-specific fixed points to be reached (3 s trials), inter-trajectory distances were greater during either of the transient phases than during the fixed points (Figure 5B).

Next, we quantified the similarity of offset trajectories between pulses of different duration. For each odor and pulse duration, we computed the mean trajectory for the first 1 s after odor offset. We found the mean distance between offset trajectories for a 1 s and a 3 s pulse of different odors is 60% greater than the mean distance between a 1 s and a 3 s odor pulse of the same odor. The same measure calculated for 300 ms and 1 s pulses is 30% and for 300 ms and 3 s pulses is 20%.

The trajectories corresponding to individual trials showed some variability around the mean trajectory (Figure 4D). To test whether the interodor distances were significant relative to this intertrial noise, we measured mean trial-to-trial distances, both within and across odor trial groups (Figure 5C). We observed that for all odor-pulse durations, interodor distances rose substantially above baseline levels, with peaks once again during the transient phases of the population response. Within-odor, intertrial distances, however, decreased below baseline noise during the transient response phases (Figure 5C), indicating that the trajectories during
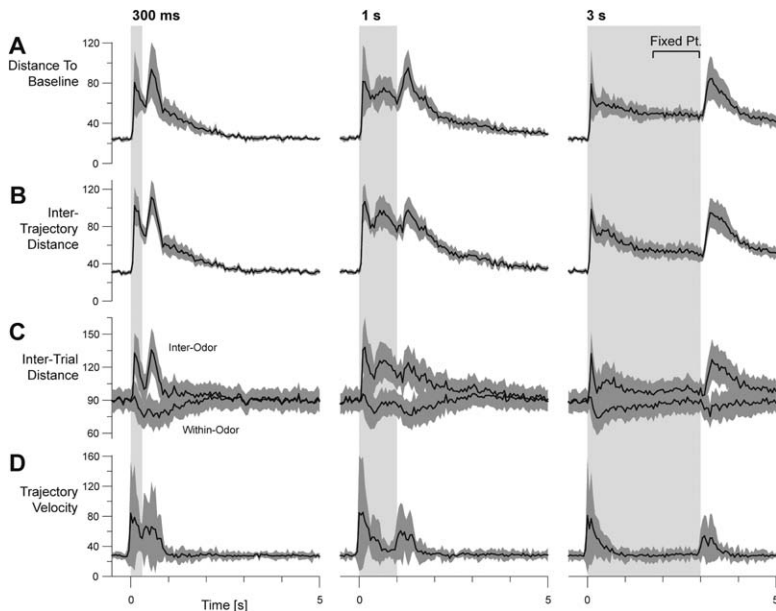
Figure 5. Quantification of Intertrajectory Distances

All distances are computed as Euclidian distance in 99-dimensional space. (A) Instantaneous distance between mean odor trajectory and mean baseline state (averaged over the five odors). Baseline state is computed from a 4 s average of preodor activity. (B) Instantaneous distances between mean odor trajectories (mean computed pairwise across all five odors). (C) Mean instantaneous trial-to-trial distances, computed pairwise across all trials from different odors (top traces) and within the same odor (bottom traces). Note that throughout the odor response, mean intertrial distances across odors are substantially higher than within odor distances. (D) Instantaneous velocity of mean odor trajectories (average over five odors). (A–D) All traces are computed in 50 ms nonoverlapping bins. Gray shading represents ± 1 SD of mean.

the dynamic phases of PN activity are less variable than either fixed point (baseline or odor evoked). Taken together, these data indicate that stimulus identification with instantaneous PN activity vectors should be most accurate during the dynamic phases of the PN-population response.

Using these measures of activity, we next estimated the rate at which the PN vectors change over time. For every 50 ms time bin, we calculated the instantaneous velocity of the ongoing trajectory by measuring the distance from that point to the point 100 ms later. Figure 5D shows the mean and SD of this estimated velocity, sampled over the five odors. We found that the evolution of the PN vectors was faster at odor onset than at offset and that velocity returned to baseline levels (e.g., the system reached a steady state) within ~1.5 s of odor onset in the case of a 3 s long stimulus.

Odor Discrimination with Single Trials
PN activity in response to multiple trials of one odor varied slightly from trial to trial (Figures 1A and 4D). Our goal here is to assess the effect of this intertrial variability on odor discrimination with instantaneous single-trial activity. We thus measured, for each odor (*cis*, *cit*, *hex*, *meth*, and *oct*), pulse-duration condition (0.3, 1, and 3 s), trial (2–10), and 50 ms time bin, the instantaneous PN vector characterizing the state of the 99 PNs. We show the PC projections of a subset of these vectors, calculated for four separate time bins: during baseline, 300 ms after odor onset, 2.35 s after odor onset (only for 3 s long odor pulses), and 350 ms after odor offset (Figure 6A). We then classified each PN vector on the basis of its distance to the cluster centers of all five odors for the corresponding time bin (see Experimental Procedures). One can see, for example, that the *cis* (orange) and *hex* (cyan) vectors overlapped during the fixed-point period (third panel, Figure 6A) but were well separated at odor onset and offset (second and fourth panels, Figure 6A). Interestingly, these two odors are chemically similar.

The percentage of correctly classified instantaneous PN vectors (over 45 individual trials—nine trials per odor × five odors) is plotted in Figure 6B, time bin by time bin, for each of the three odor durations. The dashed lines indicate chance level (20%, given five odors). For all three odor pulse durations, the percentage of correct classification was at chance level at baseline, rose to almost 100% within 100–150 ms after onset and decayed back to chance some time after odor offset, at rates correlated with the duration of the preceding pulse (the shorter the pulse, the faster the return to chance-level classification). Correct classification remained close to 100% throughout the 0.3 and 1 s odor pulses and at the beginning of the dynamic phase after odor offset. Correct classification rates fell to ~80% toward the middle of the 3 s responses. This corresponds to the times when odor-specific fixed points are reached and when distances between odor trajectories are reduced (Figure 5B).

We then used this classification method to test the temporal sensitivity of the odor representation: specifically, we examined how the rate of successful classification of PN activity vectors (measured in one time bin) degrades as the classification templates are taken from time bins further and further away from that of the test vector. Figure 6C represents classification success (color look-up table) as a function of time (x axis) and of temporal offset between test and template vectors (y axis). Offsets between −500 ms and +500 ms were examined, in 50 ms increments. At zero offset (y = 0) (Figure 6C), classification success corresponds to the plots in Figure 6B. The thickness or width of the blue band (see box, Figure 6C) thus represents the temporal sensitivity of the PN-population odor representation. This width was averaged over the first 1 s of the PN-ensemble response (300 ms odor pulse, five odors, 20 successive 50 ms bins) and plotted in Figure 6D. Throughout this 1 s period, the average successful classification rate with no offset between test and template is 96.9% (SD: 4.52). With temporal offsets of ± 150 ms (that is, with template
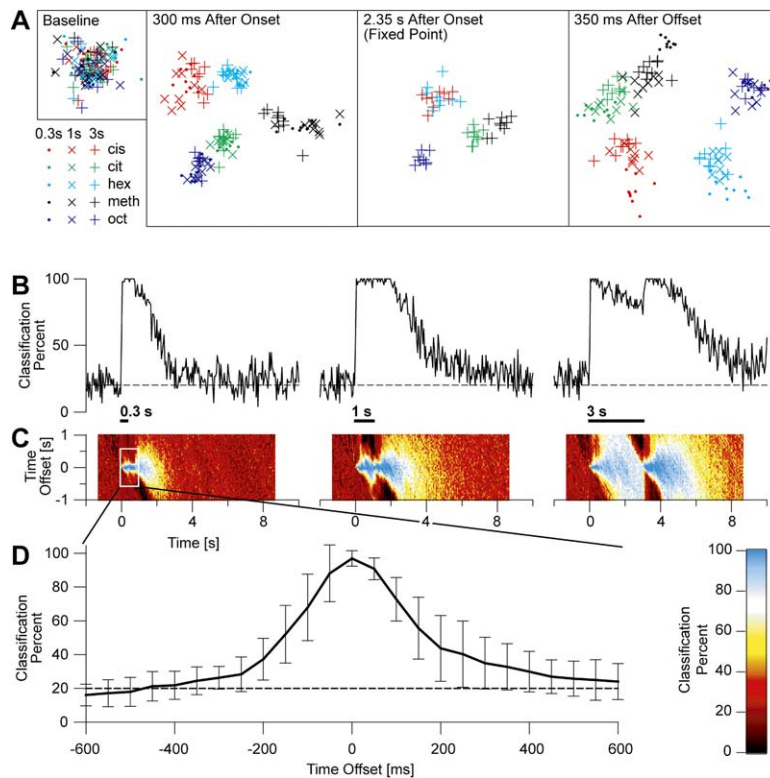
Figure 6. Odor Information Is Available from 100 ms Time Slices of Single Trials, and Discriminability Is Highest during Transient, Dynamics Phases

(A) The activity of the PN population captured at four different time points (100 ms bins): baseline (preodor), 300 ms after odor onset, 2.35 s into the response (3 s odor only), and 350 ms after odor-pulse offset. The first two principal components are displayed, computed separately for each time bin. Each marker represents the PN-population activity (spike count in 100 ms) from a single trial of one odor. Note that individual odors form generally nonoverlapping clusters and vectors cluster by odor, relatively independent of odor pulse duration.

(B) Odor classification percentage over time, based on single-trial, 99-PN vectors in 50 ms time bins (see Experimental Procedures).

(C) Odor classification percentage over time with temporal offset between test and template vectors. The pixels at y = 0 correspond to the plot in (B).

(D) Effects of time offset between test and template vectors (vertical section through the plot in [C]) on classification percentage, averaged over first 1 s of response to 300 ms odor pulse. Classification success of PN vectors with templates taken at different times decreases rapidly with time offset.

vectors at time t to classify PN vectors at time t ± 150 ms), however, successful classification rate dropped to 55.7% and 52.0%, respectively (SDs: 18.3, 17.1). This shows how quickly the PN activity vectors evolve over time: a few oscillation cycles (50 ms long each on average) are therefore sufficient time to decorrelate PN-activity vectors with themselves enough to hinder odor identification with intervector distances.

Local Field Potentials
The dynamical PN response patterns examined above occur on top of faster periodic (20–30 Hz) synchronizing events across the PN populations (Laurent and Davidowitz, 1994; Wehr and Laurent, 1996). During an odor response, individual PNs are thus transiently synchronized with other PNs, in an odor-specific manner. Following our analysis of PN-response evolution over time (above), we study here how synchronization across the PN population evolves during an odor response. For this portion of the analysis we will focus primarily on data from 1 s long odor pulses.

LFPs (Figure 7A) are typically recorded with extracellular electrodes from the Kenyon cell body cluster, dorsal to the mushroom body calyx. These LFPs are thought to result mainly from the alternating excitatory and inhibitory synaptic currents generated in Kenyon cells (the targets of PNs in the mushroom body) by PNs and lateral horn interneurons, respectively (Perez-Orive et al., 2002).

We measured the average LFP power (in the 10–30 Hz band) as a function of time around an odor pulse. Power was calculated with a scrolling window (width 200 ms, step 50 ms) over all trials (ten per stimulus condition) and odors (five) and averaged over ten mushroom bodies. This average is plotted for a 1 s odor pulse, together

with a typical single-trial LFP trace (Figure 7A). The single trial illustrates that short bouts of synchronization occur throughout baseline but that the dominant power emerges right after odor pulse onset. Mean oscillatory power reached a peak within about 300 ms of PN-population activation onset and decreased in two successive phases: the first occurred within the first 1 s of the odor pulse, and the second, after odor offset. This was true for 3 s odor pulses as well. The period of peak oscillatory power thus corresponds to the dynamic phase when the PN-population vector evolves away from baseline but before it reaches its odor-specific fixed point (Figures 4 and 5).

Because all the PNs were recorded simultaneously with an LFP, we could attribute a phase to all the PN spikes that occurred when 20 Hz oscillatory power was significant (see Experimental Procedures). Figure 7B shows the distribution of PN spike phases, calculated at different epochs before, during, and after the odor pulse. The phase distributions are all shifted vertically (dark gray boxes at the bottom) by an area corresponding to the number of spikes for which phase could not be attributed (because of insufficient 20 Hz power). At rest, PN spikes showed a small degree of phase locking to the rising phase (180°–360°) of the LFP oscillations. During the odor response itself, PNs were strongly phase locked to the rising phase of the LFP oscillations (mean phase, 290°). The preferred phase of PN firing relative to the LFP remained roughly constant. By computing similar phase histograms for every time bin and odor trial, we constructed a 2-dimensional histogram (Figure 7C) representing the relative number of spikes attributed to each phase over time (y, 18° steps; x, 50 ms steps). It shows that in the 1 s after odor onset, the total number
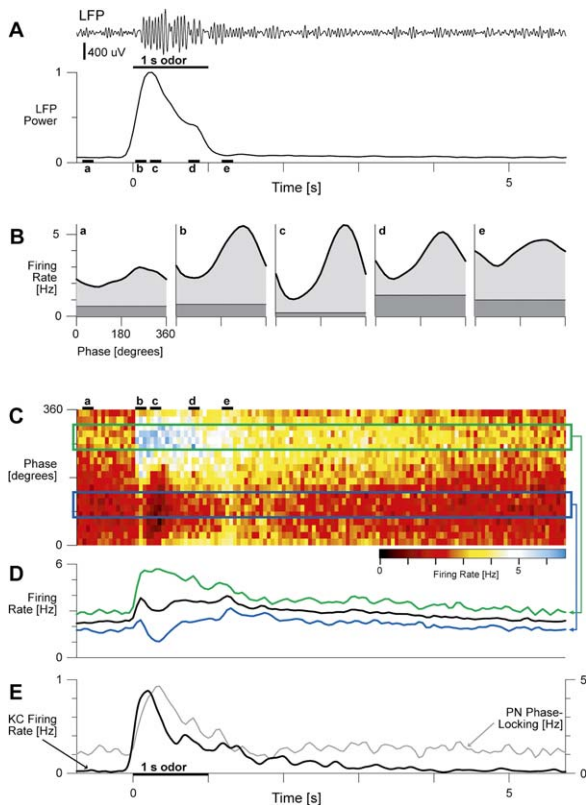
Figure 7. KC Population Activity Best Matches Period of Peak PN Synchronization

(A) Single-trial LFP response (upper trace, bp filtered 10–30 Hz) and mean normalized LFP power in 10–30 Hz band (lower trace, mean over five odors and ten recording sessions, 200 ms sliding window). Both traces for 1 s odor duration.

(B) Phase alignment histograms for PN spikes with respect to the LFP, computed at five different time points (150 ms bins, at times indicated in [A]) during the response. Each phase distribution rests on a pedestal (dark gray box) that corresponds to the number of PN spikes for which phase could not be attributed (because of insufficient 20 Hz power).

(C) Two-dimensional histogram of PN spike phase over time in response to a 1 s odor pulse. Each column represents a 50 ms time bin. The values along the column are the histogram of all PN phases (with respect to the LFP) recorded during that time bin.

(D) Comparison of response strength for PN spikes of different phase alignments. Green trace (top), mean firing rate for spikes locked to the preferred phase of the LFP. Blue trace (bottom), mean firing rate for spikes locked to the nonpreferred phase of the LFP. Black trace (center), mean firing rate for all spikes. Spikes with phases within 36° of 290° (90°) were considered locked to the preferred (nonpreferred) phase. Firing rate for phase-aligned spikes represents probability of spiking within the preferred (nonpreferred) portion of the cycle.

(E) Mean Kenyon cell firing rate (black) in response to a 1 s odor stimulus (n = 20 KCs, six odors). The profile of PN phase-locking strength (the difference between the green and blue curves in [D]) is plotted in gray. The Kenyon cell firing profile shows a strong fit to this measure of PN behavior.

of spikes with phases around 290° (rising phase) increased sharply. Furthermore, there was a transient decrease in spikes with phases between 0° and 180° (falling phase) during the first 300 ms of the response. We next considered only those spikes with phases within 36° of the mean preferred phase (290°) and measured their instantaneous rate of occurrence over time. Simi-

larly, we measured the occurrence rate of all spikes falling within 36° of the mean nonpreferred phase (90°). Both measures are plotted in Figure 7D (green and blue), along with the mean PN firing rate (black).

Kenyon Cell Responses

We examined whether the detailed statistics of the PN-population output could help identify those features of the PN response that are most likely to drive a KC to respond. We showed previously that KCs are tuned to detect synchronous inputs, thanks to a combination of intrinsic properties and delayed feed-forward inhibition that decrease the KCs' integration time constant (Perez-Orive et al., 2002, 2004). Feed-forward inhibition is phase locked to PN output (thus to the LFP) and follows it with a half-cycle delay (Perez-Orive et al., 2002). We thus hypothesized that Kenyon cell activity might correlate not only with mean PN firing rate but possibly better with PN oscillatory coherence.

We thus recorded from Kenyon cells and compared the temporal profile of their mean firing rate (1 s odor pulses) (Figure 7E) with several potentially relevant statistics of the PN-population response. We first considered the 2 s period after odor onset, which includes 85% of odor-evoked Kenyon cell spikes. During this time, the mean PN firing rate increased by 44% over baseline. In contrast, the rate of PN spikes at the preferred phase (Figure 7D, green trace) increased by 57% over baseline. We next defined PN phase-locking strength as the difference between the occurrence rates of preferred-phase and nonpreferred-phase PN spikes (i.e., the difference between the green and blue traces in Figure 7D). This quantity (Figure 7E) increased by 111% over baseline during the same period.

To compare the time courses of these measures to the distribution of Kenyon cell-response probabilities, we computed the correlation coefficient (Pearson's coefficient, zero lag) between the mean Kenyon cell firing rate (Figure 7E) and each of the previous three PN statistics (in 50 ms time steps over 3 s after odor-pulse onset). The correlations were 0.83 with either phase-locked PN spike rate or PN phase-locking strength, compared to 0.43 with mean PN firing rate.

Finally, we tried to identify the epochs of the PN-population response—onset dynamic phase, offset dynamics, or fixed point—that best evoke spiking in the KCs (those epochs should be the most relevant ones for olfactory processing). In response to 1 s odor pulses, KCs showed a detectable increase in firing over baseline for ~4 s (Figure 7E), although most Kenyon cell spikes occurred over the 1–2 s after odor onset. To help separate the relevance of the three epochs of the PN-population response, we also recorded the responses of Kenyon cells to 10 s long odor pulses. Across recordings from 20 Kenyon cells and six odors, the mean firing rate in the 1 s after odor onset was 0.49 spike/s. It was 0.24 spike/s in the 1 s after odor offset, and only 0.059 spike/s over the last eight seconds of the 10 s odor pulses. This rate, obtained during the odor-specific fixed point, was not substantially different from the baseline (preodor) rate of 0.045 spike/s, indicating that even though the fixed points are odor specific, PN output at steady state produces little, if any, response across the Kenyon cell population.
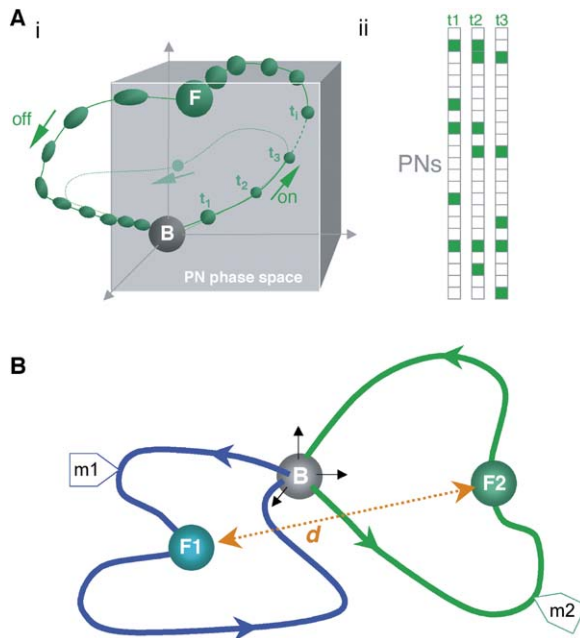
Figure 8. Schematic Diagram of Odor-Evoked PN Activity

(Ai) Idealized odor trajectory in PN space. *B*, baseline; *F*, fixed point; *t_i*, times corresponding to one oscillation cycle. During the on transient, synchronization is the highest and most spikes occur within a single 10–20 ms period. Activity thus "hops" from one oscillation cycle to the next while the identities of the responding PNs evolve (see [Aii]).

(Aii) Evolving PN activity that underlies the trajectory in (Ai), green squares represent responsive PNs.

(B) Idealized trajectories for two different odors. Odor trajectories differ at their fixed points (*F1* and *F2*) but are maximally distant during the transient response phases (e.g., *m1* and *m2*). (d, Euclidian distance.)

Discussion

PN-Population Responses to Odors as Trajectories in Phase Space

The systematic study of 99 locust antennal lobe projection neurons within a population of about 800 gives us the most precise picture so far of the collective behavior (response distributions and time course) of this system during an odor stimulus. To facilitate its description, we measured the state of the PN ensemble as time series of PN activity vectors, measured over short, successive time bins. This strategy was critical to capture the evolution of this highly dynamical system. Our time bin was typically 50 ms, for reasons that will be examined later. The main results can be summarized as follows.

At baseline, individual PNs fire at an average rate of about 2.6 spikes/s. When represented in PN state space, baseline for all odors corresponds to a hypersphere of noise in the neighborhood of a fixed origin (*B*, Figure 8A). Shortly after odor-pulse onset, activity spreads across the PN population, in a manner that depends on the duration of the stimulus. With long odor pulses ($\geq$ 3 s), PN activity is characterized by three successive phases. (1) An onset transient (*on*, Figure 8A), when activity evolves rapidly across the PN population and is highly coherent; this phase can be represented geometrically as a stimulus-specific trajectory in PN state

space. (2) After 1.5–2 s, an odor-specific fixed point is reached (*F*, Figure 8A); PN responses cease to evolve and oscillatory synchronization decreases. Stability persists for at least 10 s if the stimulus is maintained. This phase is consistent with recent calcium-imaging experiments in the antennal lobe of honeybees, suggesting the existence of odor-specific fixed points (Fdez Galan et al., 2004). (3) After odor-pulse termination, we observe a second transient (*off*, Figure 8A), during which PN activity becomes dynamic again, with reduced oscillatory synchronization relative to the on transient, and finally relaxes to baseline at decreasing velocity. The on and off transients are always different from one another, yet both are odor specific.

With shorter odor pulses, the segments corresponding to an odor-specific fixed point (or to the approach to it) are never experienced; the trajectories then consist of joined on and off transients, with diminishing excursions as the odor pulses become shorter. The off transients after different duration pulses of the same odor generally converge before reaching baseline. No steady state is ever reached for odor pulses lasting 1 s or less; their representations across the PN population are thus always nonstationary. In such conditions, the onset and offset transients retain their identity, even though they merge together to form one continuous response loop, to and from baseline. The shorter the stimulus, the shorter the loop. Trial-to-trial variability of the instantaneous PN activity vectors is less during either transient than it is at rest or at an odor-specific fixed point. We now examine the significance of these results.

Results versus Winnerless Competition Dynamical Framework

Recent theoretical work by Rabinovich and colleagues (Laurent et al., 2001; Rabinovich et al., 2001) proposed a nonlinear dynamical systems framework to describe odor-evoked PN activity. In this framework, called winnerless competition (WLC), PN activity can be thought of as stimulus-specific orbits in PN phase space: these trajectories are defined by sequences of unstable attractors (saddle states), that each correspond to the activation of a specific subset of synchronized PNs. The attractors are the trajectories (heteroclinic orbits) themselves. They are very sensitive to the input but globally stable: small individual-neuron deviations are corrected at the next step by the distributed and stabilizing effects of the population. When the input is withdrawn, the system relaxes back to the origin (baseline). Our present results reveal a deviation from the predictions of the initial WLC model: the existence of odor-specific fixed points for long odor-pulse duration. Although WLC dynamics may still explain the transient portion of the PN-population response (Afraimovich et al., 2004), a modification of this framework—or another framework entirely—may be needed to account for fixed-point response.

How Should One Decode the PN Trajectories?

PN activity vectors have no opportunity to stabilize at odor-specific fixed points under many natural circumstances (short intermittent odor pulses, as are typical in odor plumes). Average-rate measurements of PN responses, calculated over hundreds of milliseconds, are therefore inappropriate. An obvious question then

arises: if the PN vectors evolve, what is the appropriate time step over which the trajectories should be analyzed? To answer this question, we turned to the PNs' own targets, the Kenyon cells, because they are the natural decoders of PN activity. Both their connectivity to the PN population and their integrative properties helped us define the relevant spatio-temporal scales for analysis.

We chose an analysis window of 50 ms because it captured the mean rate of collective PN output (20 Hz, as measured by the LFP or from the membrane potential of KCs during odor responses) while not confounding potentially faster evolution of PN output: indeed, we know from previous work (Laurent et al., 1996; Wehr and Laurent, 1996) that PN spike phase (relative to the global 20 Hz output) does not vary with stimulus conditions. Although it is longer than the typical window over which synchronized PN output occurs (about 10–20 ms), the 50 ms window captured the fastest stimulus-specific evolution of the PN-population output.

Kenyon-Cell-Response Probability Profiles Point to the Code across PNs

Kenyon cells are the PNs' targets in the mushroom body: they can therefore be used as a direct assay for the functionally relevant components of the PN-population response, perhaps even more directly than behavioral assays could. In the locust, each KC receives inputs from an estimated 400 PNs on average (R.A. Jortner, S.S. Farivar, G.L., unpublished data) and yet hardly ever fires at rest and responds to very few odors (Perez-Orive et al., 2002). In the mushroom body, odors are thus represented by assemblies of specific neurons representing a small fraction of the KC population (Laurent, 2002; Perez-Orive et al., 2002, 2004; Stopfer et al., 2003). This specificity is proposed to result from a combination of synaptic and cellular properties of KCs, feed-forward inhibitory circuits, connectivity, and from the statistical structure of PN output (Perez-Orive et al., 2002, 2004).

We noted that the proportion of reliable PN spikes (i.e., those that occurred in the same 50 ms bin in at least six of nine different trials with the same stimulus) during the odor response was only about 55%. These spikes come from an evolving population of about 10% out of the ~800 PNs in the locust antennal lobe. Because 60% of PNs (~480) are silent at this time, the remaining 45% of spikes must come from a less-reliable set of ~240 PNs. This means that for each time bin, i, a small number of KCs could receive input from all (or most) of the 80 PNs that reliably respond to odor A as well as from many of the 240 less-reliable PNs (by virtue of the input connectivity of these KCs). Such KCs would receive maximal input at time bin i during the response to odor A in any trial, regardless of which of the less-reliable PNs fired in each trial. At all other time bins in response to odor A and at all times during the responses to other odors, the input to this KC would be submaximal. This is because some of the reliable PNs at time i become unreliable or silent at other times during the response. For example, a KC that receives inputs from PNs 1–25 in Figure 3 (out of a sample population of 99) would be maximally excited 300 ms after the onset of odor 1. It would receive substantially less input 50 ms later and even less excitatory input at other times or to other odors. In this way, the temporal dynamics of the

PN-population response can underlie the high degree of stimulus and temporal specificity described in KC's responses (Perez-Orive et al., 2002, 2004; Stopfer et al., 2003). This also means that a KC can tolerate that a large proportion of its inputs be unreliable, even at the time when its response is the most reliable. This was first noted (to our knowledge) in this context by Kanerva (1988) in his mathematical exploration of sparse distributed memories in networks of binary units. Highly distributed connectivity reduces overlaps between input vectors, which in turn ensures that high response specificity can be achieved by combining two sets of inputs: ones that are highly reliable in origin (they confer input specificity) and ones that are highly reliable collectively, but whose precise origin is unimportant (they ensure that firing threshold can be crossed). This circuit design thus confers resistance to noise even though only a portion of the inputs to a specific neuron are required to be reliable.

By measuring the instantaneous firing-rate profiles of Kenyon cells over the same odors as used with PNs, we found here that KC response probability, averaged over all KCs and odors, show a weak correlation with PN instantaneous firing rates and a much stronger correlation with instantaneous PN oscillatory coherence (in the 20 Hz band). These results are consistent with the idea that the rise in PN synchronization after odor onset is largely responsible for the increase in total KC population activity, whereas the extreme specificity of KC responses are due to the odor-specific dynamics of the PN population.

The antennal lobe code for odors thus consists of vectors of PN activity, updated once per oscillation cycle. Over a single trial and during the response phase that corresponds to peak KC activity, PN activity evolves so rapidly that classification of PN activity vectors measured at one time against templates measured five cycles earlier or later is no better than chance (Figure 6). This rapid evolution helps explain the temporal specificity often observed with individual KC responses (Perez-Orive et al., 2002, 2004): because KCs receive a strong voltage reset (IPSP) in the second half of each oscillation cycle (Laurent and Naraghi, 1994; Perez-Orive et al., 2002), temporal integration across successive cycles is limited or prevented. KCs thus each decode PN activity vectors one oscillation cycle at a time. The limited width of PN-vector correlation (the limited time over which PN activity vectors remain sufficiently self similar) explains why KC response times should be narrowly distributed.

Similarly, we observed that KC firing probability was very close to zero when the PN-population response had reached its odor-specific fixed point. This time corresponds to that when PN output is least synchronized, consistent with the above conclusion. We note, however, that olfactory classical conditioning studies in honeybees (Bitterman et al., 1983; Kuwabara, 1957; Menzel and Müller, 1987; Stopfer et al., 1997) generally use a conditioning paradigm consisting of a 4 s odor pulse overlapping with a sugar reward only after the first second of the odor pulse onset. This suggests that the unconditioned stimulus is often presented once PN responses reach their fixed point (after ~1 s in honeybees) (Fdez. Galan et al., 2004)—well after the onset transient when odor representations in locust PNs are maximally informative and KC activity is most likely. This temporal

offset raises interesting question about the mechanisms that underlie the association of the conditioned and unconditioned stimuli within the mushroom body.

When Are PN Activity Vectors Most Informative?

PN instantaneous firing rates averaged over the entire population increased by only ∼1.5 spikes/s relative to baseline at the peak of the population odor response. What changed most was the variance of instantaneous firing rates across the population. The periods of peak variance were also those when vector classification was the most reliable. Indeed, a result most surprising to us was that peak separation of instantaneous PN activity vectors (averaged over trials) did not occur at the odor-dependent fixed points, but rather sometime during the dynamic phases of a response. Trial-to-trial variations were also smaller during the dynamic phases than at the fixed points. For example, two related alcohols could not be distinguished from their corresponding instantaneous PN vectors at the fixed point but could be separated during the on and off transients. Our results indicate that the PN activity vectors (especially with single trials) are most informative during the dynamic phase immediately after odor onset and odor offset. These periods last several hundred milliseconds (estimated over this data set), but near perfect discrimination was reached as early as within 100–150 ms. The onset transient period is characterized by peak PN synchronization, and both transients show peak firing-rate variance across the PN population, fastest rate of PN-vector evolution, and lowest intertrial variability.

Do locusts take advantage of these periods of maximum odor discriminability? Behavioral evidence from other insects suggests that the minimum reaction time to an odor is in the range of 200–500 ms in the best case and can often be much longer. Moths will modify their flight patterns ∼300–400 ms after entering or leaving a pheromone plume (Vickers and Baker, 1996). Similar best-case reaction times are observed in mammals, in which highly trained rodents can discriminate odors within ∼300 ms of odor presentation (Abraham et al., 2004; Uchida and Mainen, 2003). Reaction times can be much longer for untrained animals, including humans, and nonpheromonal odors (Livermore and Laing, 1996). Our results are thus consistent with behavioral data on fastest olfactory reaction times.

Because these highly informative periods are both transient and dynamic, they are unlikely to be detected by measures of neural activity with low temporal resolution (e.g., slow calcium indicators in insects or intrinsic signal imaging and fMRI in mammals). Rather, these techniques are more likely to detect the steady-state response to long odors, which we show to be less informative and functionally less relevant in this system. This concern is by no means unique to the locust olfactory system and might apply to many other systems in which dynamics have been observed (Aksay et al., 2001; Buzsaki and Draguhn, 2004; Freeman, 2000; Hahnloser et al., 2002; Mao et al., 2001; Skaggs and McNaughton, 1996).

Does the Antennal Lobe Encode Olfactory Changes?

As described above, the periods of peak odor discriminability of PN activity arise in response to changes in the olfactory environment. The PN population also eventually exhibits odor-specific steady-state responses to prolonged odor pulses, but these steady states are less informative about the odors than either the onset or offset transients; more importantly, unlike both transient responses, PN steady-state output elicits almost no activity from the KC population. Thus, the locust olfactory system seems to be selective for temporal variations of its input. The detection of odor onset and offset transitions is probably ethologically critical because natural odor plumes consist of filaments of concentrated odor intertwined with relatively clean air with sharp transitions in between (Murlis et al., 1992). The importance of intermittent odor stimuli has been demonstrated in moths, which will follow a pulsing pheromone stimulus upwind but not a continuous pheromone stream (Vickers and Baker, 1994). Sensitivity to transitions seems to be an underlying principle across many sensory modalities. Neurons in the early visual system act as high-pass filters in both space and time (Juusola et al., 1996; Meister and Berry, 1999), and neurons in auditory cortex can show strong transient responses to acoustic stimulation (Phillips, 1985; Wang et al., 2005). The current results show that the locust olfactory system is also tuned to changes in the sensory environment and that these transient responses are themselves composed of odor-specific dynamics.

Experimental Procedures

Preparation and Stimuli

Results were obtained from locusts (*Schistocerca americana*) in an established, crowded colony. Young adults of either sex were immobilized, with one or two antennae intact for olfactory stimulation. The brain was exposed, desheathed, and superfused with locust saline, as previously described (Laurent and Naraghi, 1994). Odors were delivered by injection of a controlled volume of odorized air within a constant stream of desiccated air. Teflon tubing was used at and downstream from the mixing point to prevent odor lingering and crosscontamination. Odors were used at 1% of saturated vapor pressure (PNs) or 10% of saturated vapor pressure (KCs) and further diluted in the dessicated air stream. Ten trials of each odor were delivered for each of four different odor durations (300 ms, 1 s, 3 s, and 10 s). The first trial of each set of ten was excluded from analysis of response activity and odor classification (Figures 2–6) to minimize the effects of short-term response plasticity (Stopfer and Laurent, 1999). For each odor, trials of 300 ms and 1 s duration were interleaved, followed by all ten trials of 3 s duration. Similarly, 1 s and 10 s trials were interleaved. Odor onset (t = 0) was defined as 250 ms after the olfactometer was triggered to deliver an odor pulse to account for the delay induced by the odor delivery system. Across all experiments, no electrophysiological response was ever observed prior to this time. Odors presented and their abbreviations are as follows: cis-3-hexen-1-ol (*cis*), citral (*cit*), 1-hexanol (*hex*), methyl salicylate (*meth*), and 1-octanol (*oct*).

Electrophysiology

Extracellular recordings were performed with silicon probes generously provided by the University of Michigan Center for Neural Communication Technology (http://www.engin.umich.edu/facility/cnct/). Custom-built 16-channel preamplifiers and amplifiers were used for the recordings. Two tetrodes were used simultaneously. The preamplifier has a unitary gain, and the amplifier gain was set to 10,000 ×. Data from the four channels of each tetrode were filtered (custom-built amplifiers, band-pass filter, 0.3–6 kHz [for PNs and KCs]; 1–300 Hz [for LFP]; and 1 Hz–6 kHz [for simultaneous KC and LFP channels]), continuously acquired (15 kHz/channel, 12 bit), and stored to disk. For PN recordings, tetrodes were placed within the antennal lobe soma clusters, peripheral to the neuropils at depths less than

200 μm. During MB recordings (KCs, LFP), probes were either pressed on the surface of the MB or placed within the KC soma clusters, peripheral to the neuropils at depths less than 200 μm. Cell identification was unambiguous because PNs are the only spiking neurons in the locust antennal lobe (local neurons do not produce sodium action potentials in locust) (Laurent and Davidowitz, 1994) and because all the somata located above the MB calyx belong to KCs.

Tetrode recordings were analyzed as described in Pouzat et al. (2002). Briefly, events were detected on all channels as voltage peaks above a preset threshold (usually 2.5–3.5 times each channel's SD). For any detected event on any channel, the same 3 ms window (each containing 45 samples) centered on that peak was extracted from each one of the four channels in a tetrode. Each event was then represented as a 180-dimensional vector (4 × 45 samples). Noise properties for the recording were estimated from all the recording segments between detected events, by computing the auto- and crosscorrelations of all four channels. A noise covariance matrix was computed and used for noise whitening. Events were then clustered with a modification of the expectation maximization algorithm. Because of noise whitening, clusters consisting of, and only of, all the spikes from a single source should form a Gaussian (SD = 1) distribution in 180-dimensional space. This property enabled us to perform several statistical tests to select only units that met rigorous quantitative criteria of isolation (Pouzat et al., 2002). A total of 99 PNs were recorded from ten antennal lobes in nine different locusts. In a separate set of experiments, a total of 20 KCs were recorded from five different locusts.

Data Analysis

All data analysis was performed with Igor Pro (WaveMetrics, Lake Oswego, OR) or Matlab (The MathWorks, Natick, MA). Our response metric was computed by taking spike time data from each PN, odor, and duration and dividing data into successive, nonoverlapping 50 ms bins. For each bin, the number of trials (excluding the first trial, see above) with at least one spike was computed. A PN was considered "responsive" at that time bin if this count reached at least six (out of nine total trials). The duration of a response was defined as the number of consecutive responsive 50 ms bin for one PN and one odor. Mean response duration was computed for each time bin, based on the response duration of all PNs responsive at that time.

Population trajectories were computed for each odor and stimulus duration as a series of vectors representing the state of the system over the course of an odor-delivery trial. The vector representing the instantaneous state of the system was computed in successive, nonoverlapping 50 ms bins. In each time bin, a 99-dimensional vector was generated in which the value of the nth dimension was the firing rate of the nth PN. For single trial trajectories, instantaneous firing rates were computed from the PN's spike count in that time bin. For mean trajectories, firing rates were computed by taking the mean single-trial firing rate across all nine trials of an odor presentation.

Principal component analysis (PCA) was performed using Matlab's Statistics Toolbox in order to display the 99-dimensional activity vectors and trajectories. For the plots in Figure 4, principal components (PCs) were computed based on all activity vectors from 300 ms before odor onset to 5 s after odor onset, from one odor (Figures 4A, 4B, and 4D) or two odors (Figure 4C) and from the 3 s odor duration (Figures 4C and 4D) or all three odor durations (Figures 4A and 4B). In Figure 4, the first three PCs captured between 25% and 31% of the total variance. In Figure 6, the first two PCs captured 9% of the baseline variance and between 28% and 44% of the variance at the other time points.

Odor trials were classified separately for each odor duration, based on the instantaneous population activity vectors calculated on 50 ms bins. In each time bin, the centroid of activity for each of the five odors was computed by calculating the mean activity vector across the nine trials of each odor. Next, for each trial and each odor, the distance from each single-trial population vector to each centroid was computed. Individual vectors were attributed to the odor with the nearest centroid in the corresponding time bin. The trial being tested was always excluded from the calculation of centroids.

Each PN spike was assigned a phase with respect to the simultaneously recorded LFP with a simple algorithm to compute spike-phase histograms. First, the raw LFP signal from mushroom body

tetrode recordings (see Electrophysiology) was bandpass filtered from 10 to 30 Hz (nonphase-distorting Butterworth filter, built-in Matlab functions). Next, all peaks and troughs that exceeded 0.5 SDs of baseline (nonodor evoked) fluctuations were detected in the filtered LFP. Spikes were assigned a phase if they fell between a peak and a trough (in either order) and if less than 35 ms separated the peak and trough. Phase was then assigned based on a linear scaling of phase values between a peak and trough (0º–180º) or trough and peak (180º–360º). Across the entire data set, a phase could be attributed to 73% of all spikes. The remaining 27% were distributed uniformly across all phases. Phase histograms were computed with 18º phase bins and 50 ms time bins. Phase-locking strength is measured in Hz by computing the average spike count for each bin and then multiplying by a normalizing factor of 400 ([360º/18º] × [1000 ms/50 ms]). Phase measures in Figures 7D and 7E were smoothed with a 50 ms Gaussian filter (built-in Igor function). These smoothed values were used to compute the Pearson's coefficient (zero lag) with the KC PSTH (which was computed with 100 ms Gaussian smoothing). Different filter settings produced quantitatively similar results.

References

Abraham, N., Spors, H., Carleton, A., Margrie, T., Kuner, T., and Schaefer, A. (2004). Maintaining accuracy at the expense of speed: stimulus similarity defines odor discrimination time in mice. Neuron *44*, 744–747.

Adrian, E.D. (1953). Sensory messages and sensation. The responses of the olfactory organ to different smells. Acta Physiol. Scand. *29*, 5–14.

Afraimovich, V., Zhigulin, V., and Rabinovich, M. (2004). On the origin of reproducible sequential activity in neural circuits. Chaos *14*, 1123–1129.

Aksay, E., Gamkrelidze, G., Seung, H.S., Baker, R., and Tank, D.W. (2001). In vivo intracellular recording and perturbation of persistent activity in a neural integrator. Nat. Neurosci. *4*, 184–193.

Axel, R. (1995). The molecular logic of smell. Sci. Am. *273*, 154–159.

Bitterman, M., Menzel, R., Fietz, A., and Schaefer, S. (1983). Classical conditioning of proboscis extension in honeybees (*Apis mellifera*). J. Comp. Physiol. *97*, 107–119.

Buck, L.B., and Axel, R. (1991). A novel multigene family may encode odorant receptors: a molecular basis for odor recognition. Cell *65*, 175–187.

Buzsaki, G., and Draguhn, A. (2004). Neuronal oscillations in cortical networks. Science *304*, 1926–1929.

Christensen, T.A., Pawlowski, V.M., Lei, H., and Hildebrand, J.G. (2000). Multi-unit recordings reveal context-dependent modulation of synchrony in odor-specific neural ensembles. Nat. Neurosci. *3*, 927–931.

Daly, K.C., Wright, G.A., and Smith, B.H. (2004). Molecular features of odorants systematically influence slow temporal responses across clusters of coordinated antennal lobe units in the moth *Manduca sexta.* J. Neurophysiol. *92*, 236–254.

Duchamp-Viret, P., Palouzier-Paulignan, B., and Duchamp, A. (1996). Odor coding properties of frog olfactory cortical neurons. Neuroscience *74*, 885–895.

Dulac, C. (1997). How does the brain smell? Neuron *19*, 477–480.

Fdez Galan, R., Sachse, S., Galizia, C., and Herz, A.V. (2004). Odor-driven attractor dynamics in the antennal lobe allow for simple and rapid olfactory pattern classification. Neural Comput. *16*, 999–1012.

Fiete, I.R., Hahnloser, R.H., Fee, M.S., and Seung, H.S. (2004). Temporal sparseness of the premotor drive is important for rapid learning in a neural network model of birdsong. J. Neurophysiol. *92*, 2274–2282.

Fitzpatrick, D.C., Batra, R., Stanford, T.R., and Kuwada, S. (1997). A neuronal population code for sound localization. Nature *388*, 871–874.

Freeman, W.J. (2000). Neurodynamics: An Exploration in Mesoscopic Brain Dynamics (London: Springer).

Friedrich, R.W., and Laurent, G. (2001). Dynamic optimization of odor encoding by mitral cell assemblies in the olfactory bulb. Science *291*, 889–894.

Hahnloser, R.H., Kozhevnikov, A.A., and Fee, M.S. (2002). An ultrasparse code underlies the generation of neural sequences in a songbird. Nature *419*, 65–70.

Juusola, M., French, A.S., Uusitalo, R.O., and Weckstrom, M. (1996). Information processing by graded-potential transmission through tonically active synapses. Trends Neurosci. *19*, 292–297.

Kanerva, P. (1988). Sparse Distributed Memory (Cambridge, MA: MIT Press).

Kauer, J.S., and Moulton, D. (1974). Responses of olfactory bulb neurones to odour stimulation of small nasal areas in the salamander. J. Physiol. *243*, 717–737.

Kuwabara, M. (1957). Bildung des bedingten Reflexes von Pavlovs typus bei der Honigbiene, *Apis mellifica*. J. Fac. Sci. Hokkaido Univ. *13*, 458–464.

Laurent, G. (1996). Dynamical representation of odors by oscillating and evolving neural assemblies. Trends Neurosci. *19*, 489–496.

Laurent, G. (1999). A systems perspective on early olfactory coding. Science *286*, 723–728.

Laurent, G. (2002). Olfactory network dynamics and the coding of multidimensional signals. Nat. Rev. Neurosci. *3*, 884–895.

Laurent, G., and Davidowitz, H. (1994). Encoding of olfactory information with oscillating neural assemblies. Science *265*, 1872–1875.

Laurent, G., and Naraghi, M. (1994). Odorant-induced oscillations in the mushroom bodies of the locust. J. Neurosci. *14*, 2993–3004.

Laurent, G., Wehr, M., and Davidowitz, H. (1996). Temporal representations of odors in an olfactory network. J. Neurosci. *16*, 3837–3847.

Laurent, G., Stopfer, M., Friedrich, R.W., Rabinovich, M.I., Volkovskii, A., and Abarbanel, H.D. (2001). Odor encoding as an active, dynamical process: experiments, computation, and theory. Annu. Rev. Neurosci. *24*, 263–297.

Leitch, B., and Laurent, G. (1996). GABAergic synapses in the antennal lobe and mushroom body of the locust olfactory system. J. Comp. Neurol. *372*, 487–514.

Lin, D., Zhang, S.-Z., Bolck, E., and Katz, L. (2005). Encoding social signals in the mouse main olfactory bulb. Nature *434*, 470–477.

Livermore, A., and Laing, D.G. (1996). Influence of training and experience on the perception of multicomponent odor mixtures. J. Exp. Psychol. *22*, 267–277.

Macrides, F., and Chorover, S.L. (1972). Olfactory bulb units: activity correlated with inhalation cycles and odor quality. Science *185*, 84–87.

Mao, B.Q., Hamzei-Sichani, F., Aronov, D., Froemke, R.C., and Yuste, R. (2001). Dynamics of spontaneous activity in neocortical slices. Neuron *32*, 883–898.

Meister, M., and Berry, M.J. (1999). The neural code of the retina. Neuron *22*, 435–450.

Menzel, R., and Müller, U. (1987). Memory traces in honeybees. In Neurobiology and Behavior of Honeybees, R. Menzel, and A. Mercer, eds. (Berlin: Springer), pp. 310–325.

Murlis, J., Elkinton, J.S., and Cardé, R.T. (1992). Odor plumes and how insects use them. Annu. Rev. Entomol. *37*, 505–532.

Olshausen, B.A., and Field, D.J. (2004). Sparse coding of sensory inputs. Curr. Opin. Neurobiol. *14*, 481–487.

Perez-Orive, J., Mazor, O., Turner, G.C., Cassenaer, S., Wilson, R.I., and Laurent, G. (2002). Oscillations and sparsening of odor representations in the mushroom body. Science *297*, 359–365.

Perez-Orive, J., Bazhenov, M., and Laurent, G. (2004). Intrinsic and circuit properties favor coincidence detection for decoding oscillatory input. J. Neurosci. *24*, 6037–6047.

Phillips, D.P. (1985). Temporal response features of cat auditory cortex neurons contributing to sensitivity to tones delivered in the presence of continuous noise. Hear. Res. *19*, 253–268.

Pouget, A., Deneve, S., Ducom, J.C., and Latham, P.E. (1999). Narrow versus wide tuning curves: what's best for a population code? Neural Comput. *11*, 85–90.

Pouzat, C., Mazor, O., and Laurent, G. (2002). Using noise signature to optimize spike-sorting and to assess neuronal classification quality. J. Neurosci. Methods *122*, 43–57.

Rabinovich, M., Volkovskii, A., Lecanda, P., Huerta, R., Abarbanel, H.D., and Laurent, G. (2001). Dynamical encoding by networks of competing neuron groups: winnerless competition. Phys. Rev. Lett. *87*, 068102 10.1103/PhysRevLett.87.068102.

Sachse, S., and Galizia, C.G. (2002). Role of inhibition for temporal and spatial odor representation in olfactory output neurons: a calcium imaging study. J. Neurophysiol. *87*, 1106–1117.

Skaggs, W.E., and McNaughton, B.L. (1996). Replay of neuronal firing sequences in rat hippocampus during sleep following spatial experience. Science *271*, 1870–1873.

Slotnick, B., and Bodyak, N. (2002). Odor discrimination and odor quality perception in rats with disruption of connections between the olfactory epithelium and olfactory bulbs. J. Neurosci. *22*, 4205–4216.

Stopfer, M., and Laurent, G. (1999). Short-term memory in olfactory network dynamics. Nature *402*, 664–668.

Stopfer, M., Bhagavan, S., Smith, B.H., and Laurent, G. (1997). Impaired odour discrimination on desynchronization of odour-encoding neural assemblies. Nature *390*, 70–74.

Stopfer, M., Jayaraman, V., and Laurent, G. (2003). Intensity versus identity coding in an olfactory system. Neuron *39*, 991–1004.

Uchida, N., and Mainen, Z.F. (2003). Speed and accuracy of olfactory discrimination in the rat. Nat. Neurosci. *6*, 1224–1229.

VanRullen, R., Guyonneau, R., and Thorpe, S.J. (2005). Spike times make sense. Trends Neurosci. *1*, 1–4.

Vickers, N.J., and Baker, T.C. (1994). Reiterative responses to single strands of odor promote sustained upwind flight and odor source location by moths. Proc. Natl. Acad. Sci. USA *91*, 5756–5760.

Vickers, N.J., and Baker, T.C. (1996). Latencies of behavioral response to interception of filaments of sex pheromone and clean air influence flight track shape in *Heliothis virescens* (F) males. J. Comp. Physiol. [A] *178*, 831–847.

Vinje, W.E., and Gallant, J.L. (2000). Sparse coding and decorrelation in primary visual cortex during natural vision. Science *287*, 1273–1276.

Wang, J.W., Wong, A.M., Flores, J., Vosshall, L.B., and Axel, R. (2003). Two-photon calcium imaging reveals an odor-evoked map of activity in the fly brain. Cell *112*, 271–282.

Wang, X., Lu, T., Snider, R.K., and Liang, L. (2005). Sustained firing in auditory cortex evoked by preferred stimuli. Nature *435*, 341–346.

Wehr, M., and Laurent, G. (1996). Odor encoding by temporal sequences of firing in oscillating neural assemblies. Nature *384*, 162–166.

Wilson, R.I., Turner, G.C., and Laurent, G. (2004). Transformation of olfactory representations in the *Drosophila* antennal lobe. Science *303*, 366–370.